Effect of Nanoparticle Dimensionality on Fluorescence Resonance Energy Transfer in Nanoparticle–Dye Conjugated Systems

Shira Halivni, Amit Sitt, Ido Hadar, and Uri Banin*

Institute of Chemistry and the Center for Nanoscience and Nanotechnology, The Hebrew University, Jerusalem 91904, Israel

ABSTRACT

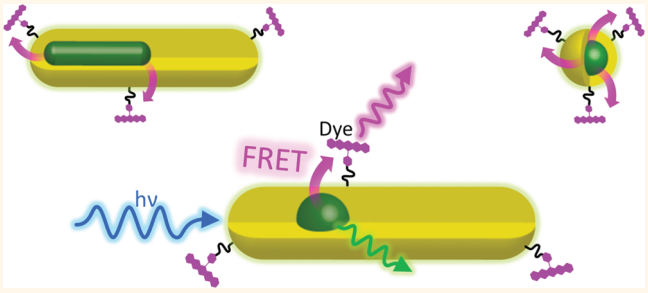

Fluorescence resonance energy transfer (FRET) involving a semiconductor nanoparticle (NP) acting as a donor, attached to multiple acceptors, is becoming a common tool for sensing, biolabeling, and energy transfer applications. Such nanosystems, with dimensions that are in the range of FRET interactions, exhibit unique characteristics that are related to the shape and dimensionality of the particles and to the spatial distribution of the acceptors. Understanding the effect of these parameters is of high importance for describing the FRET process in such systems and for utilizing them for different applications. In order to demonstrate these dimensionality effects, the FRET between CdSe/CdS core/shell NPs with different geometries and dimensionalities and Atto 590 dye molecules acting as multiple acceptors covalently linked to the NP surface is examined. Steady-state emission and temporal decay measurements were performed on the NPs, ranging from spherical to rod-like shaped systems, as a function of acceptor concentration. Changes in the NP geometry, and consequently in the distributions of acceptors, lead to distinctively different FRET behaviors. The results are analyzed using a modified restricted geometries model, which captures the dimensionality of the acceptor distribution and allows extracting the concentration of dye molecules on the surface of the NP for both spherical and elongated NPs. The results obtained from the model are in good agreement with the experimental results. The approach may be useful for following the spatial dynamics of self-assembly and for a wide variety of sensing applications.

KEYWORDS: energy transfer · semiconductor nanoparticles · core/shell quantum dots · seeded rods · organic dye · spectroscopy

Ever since the pioneering work of Förster,[1,2] fluorescence resonance energy transfer (FRET) has become a basic experimental tool extensively used in a variety of fields. Its strong dependence on distance makes FRET a "nature-made" nanometric ruler used in biological and chemical systems to determine distances on the molecular scale and as an instrument for following the dynamics of attachment processes and changes in configurations and dimensionality of systems.

The high sensitivity of FRET in the nanometric regime makes it a natural tool for investigation of systems involving nanoparticles (NPs). The use of fluorescence NPs as donors and acceptors for FRET applications is becoming increasingly common,[3−8] stimulated by the rapid development in the synthesis of colloidal semiconductor NPs and the improved ability to design and control their properties through chemical procedures. NPs are suitable for that purpose mostly because of the ability to modify their absorption and emission through size control, but also because of their high emission quantum yields (QYs), the flexibility of using different ligands as linkers for conjugation between NPs and molecular systems, and the ability to transfer them from organic to aqueous media through ligand exchange, crucial for biological usages. In particular, NPs are excellent long-lived energy donors due to their narrow emission peaks, wide and continuous absorption spectra above the band edge, and high stability under illumination.[9]

A key advantage of using NPs for FRET is the ability to connect to them several donors (or acceptors), which leads to increased FRET efficiency. FRET using NPs was utilized for a variety of applications including sensing,[5,10] biolabeling,[11−13] and energy funneling for light-harvesting devices.[14,15] Furthermore, the study of FRET properties of spherical quantum dots (QDs) in solutions and arrays is well presented in the literature. While nonspherical NPs were utilized for FRET as well, only a few studies examined the effect of NPs' dimensionality on the

* Address correspondence to banin@chem.ch.huji.ac.il.

Received for review January 16, 2012 and accepted February 7, 2012.

Published online February 07, 2012
10.1021/nn300216v

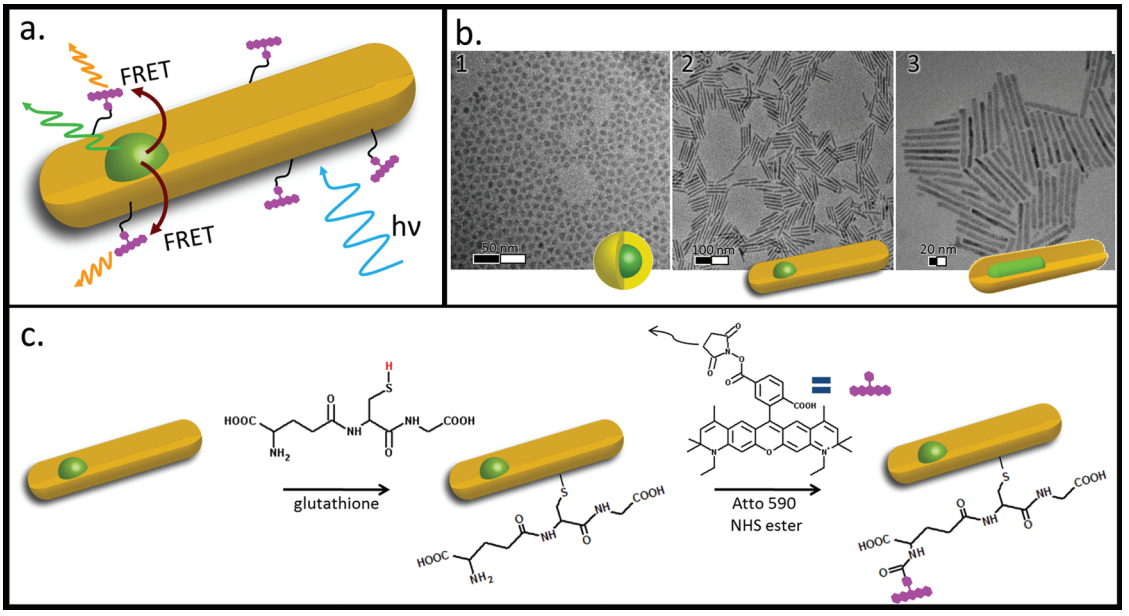

Figure 1. (a) Illustration of the FRET process in a dot in a rod conjugated system. Energy transfer occurs from the CdSe core to the dye molecules as a function of the distance. (b) TEM images of the three types of nanostructures used as donors: (1) CdSe/CdS QDs, (2) CdSe/CdS DRs, and (3) CdSe/CdS RRs. (c) Illustration of the conjugation process between the NP and the dye molecules. The first step consists in ligand exchange from the organic ligands to the water-soluble glutathione ligand. The second step consists in chemical amide bond formation between the amine group of the glutathione and the carboxylic group of the dye molecule, accompanied by the release of the dye NHS ester group.

FRET characteristics. In particular, comparisons between nanorods and spherical QDs were performed for NP and dye mixtures,[16,17] for NPs acting as acceptors,[18] and recently also for systems of dye acceptors attached to NP donors.[19] Yet, the improved ability to control the geometry, size, and morphology of highly emissive NP heterostructures that was obtained in recent years and the emerging capabilities to specifically conjugate acceptors to the surface of the NPs open new possibilities to methodically study the effect of changing the NPs' geometry and dimensionality on its FRET properties.

In this study, we explore the effects of the dimensionality and shape of NPs acting as donors on the FRET to dye molecules chemically conjugated to the NP surface, acting as multiple acceptors (see Figure 1a). We examine the steady-state emission, temporal decay, and FRET efficiency of systems consisting of CdSe/CdS core/shell NPs of different geometries and dimensions, including spherical QDs, dot in a rod (DR) structures, and rod in a rod (RR) structures. The obtained results are analyzed using a restricted geometries model, which captures the effect of the acceptors' distribution, governed by the dimensionality and shape of the NPs, on the FRET behavior of the system. Combining the model with the experimental results, we extract the acceptors' distribution and concentrations around the NP, demonstrating the power of FRET using NPs as a direct spectroscopic analytical tool for sensing. In addition, by comparing the behavior of DR systems to a RR system of similar dimensions, we study the effect of the NP emission center dimensionality on the FRET behavior, showing improved FRET efficiency when going from point dipole in DR to line dipole in RR donor.

RESULTS AND DISCUSSION

Systems Characterization and Spectroscopic Properties. In order to directly compare the effect of dimensionality, without introducing other effects, it was important to obtain NPs with close emission wavelengths but with different shapes. CdSe/CdS core/shell NPs were selected as a model system due to the developed ability to control their shape and to engineer their band gaps through synthesis parameters. CdSe/CdS core/shell NPs of different dimensionalities were synthesized, including core/shell spherical NPs,[20] DR elongated NPs in which the emission center is a spherical core,[21] and RR elongated NPs,[22] in which the emission center is an elongated rod. The NPs dimensions, obtained from tunneling electron microscopy (TEM) images shown in Figure 1b, and the spectroscopic parameters of the NPs are summarized in Table 1.

The ability to directly bind dye molecules to the surface of the NP makes NP–dye conjugates a unique system in which the NP acts not only as the donor but also as a scaffold that governs the spatial distribution of the acceptors. In order to form the conjugation, the NPs were first transferred from organic to aqueous medium, by exchanging the hydrophobic phosphonic surface ligands to hydrophilic glutathione peptide ligands, which strongly attach to the surface of the

TABLE 1. Summary of the Properties of the Different Systems Described in This Paper

particle structure	sample name	core dimensions [nm]	NP dimensions [nm]	overlap integral $\times 10^{15}$ [$M^{-1}cm^3$]	calculated R_0 [nm]
spherical core/shell	QD4.4	2.2	4.4	6.5	5.4
	QD7.6	1.9	7.6	20	6.5
dot in rod	DR45	2.2	45 × 4.6	7.1	5.5
	DR93	2.2	93 × 3.5	5.2	5.2
rod in rod	RR	9 × 2.2	40 × 3.6	13	6.0

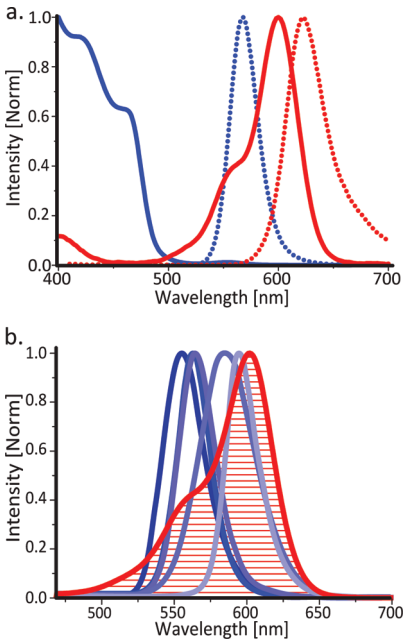

Figure 2. (a) Absorption (solid line) and emission (dotted line) spectra of DR45 (blue) and Atto 590 dye (red). (b) Emission spectra of (from left to right) DR93, QD4.4, DR45, QD7.6, and RR (blue solid lines), compared to the absorption of Atto 590 dye (red), indicating the overlap integral between the different donors and the acceptor.

NP through a thiol group without significantly quenching the emission of the NPs. Next, Atto 590 *N*-hydroxysuccinimide (NHS) ester dye in dimethylformamide was added to the NPs solution. The dye conjugates to the glutathione through the formation of an amide bond, as portrayed in Figure 1c. The conjugation procedure leads to formation of a layer of dyes with a well-defined distance from the NP surface that follows the particle's contour.

Aside from the necessary proximity between the donor and the acceptor achieved by the conjugation, an essential condition for an efficient energy transfer is a good spectral overlap between the emission of the donor and the absorption of the acceptor. Figure 2a shows, as a representative example of the NPs used as donors in this study, the absorption (solid) and the emission (dotted) spectra of the sample DR45 (in blue) and of the Atto 590 dye (in red) used as acceptor. The spectral overlap between the emission of the different NPs and the absorption of the dye is presented in Figure 2b, indicating, as mentioned above, that the emission spectra of the NPs, and hence the overlap integral with the dye absorption (summarized in Table 1), are similar. In order to minimize the direct excitation of the dye, the conjugated systems were excited at a wavelength of 470 nm, where the acceptor absorption is negligible in comparison to that of the NP donors, as can be seen in Figure 2a. Using the overlap integral, one can obtain the Förster distance (R_0) for the system, which represents the distance between the donor and a single acceptor at which the donor's radiative decay is equal to its decay through FRET. The values of R_0, presented in Table 1, are between 5.2 and 6.5 nm, in agreement with previous results.[23]

FRET in Steady-State and Lifetime Measurements. The FRET characteristics of the systems can be obtained by following two observables: the steady-state emission and the temporal decay. Figure 3 presents the steady-state emission (Figure 3 top) and the time-resolved emission traces (Figure 3 bottom) obtained for samples QD4.4, DR93, and RR (Figure 3, panels a, b, and c, respectively), mixed with different concentrations of dye, where the added dye molecules to NP ratios in solution range from 0 to 280. The overall concentration of the solutions was kept low in order to reduce the probability of FRET to unconjugated dye molecules. The presence of a FRET process is clearly evident in the steady-state emission measurements from the decrease in emission of the donor NPs, accompanied by the increase in emission of the dye acceptors, and in the time-resolved emission decay curves of the NPs, which show a decrease of the donor's lifetime. Control experiments were performed on NP–dye mixture of the same concentrations but with no conjugation. In these experiments only negligible changes in emission were observed, indicating that the FRET occurs as a result of chemical conjugation of the dye (Supporting Information, Figure S1).

Both methods indicate that the FRET increases as the dye concentrations increase. Moreover, the decay rate of the conjugated system can even exceed that of the free dye upon conjugation of enough dye molecules. While at a ratio of 125 dye molecules added per NP, the emission from QD4.4 is almost completely quenched, for DR93 NPs such a quench was not obtained even at higher ratios of dye per NP. Assuming that the number of dye molecules attached to the NP is dictated by the amount of dye added per NP, the lower quenching for the DR system under a similar amount of

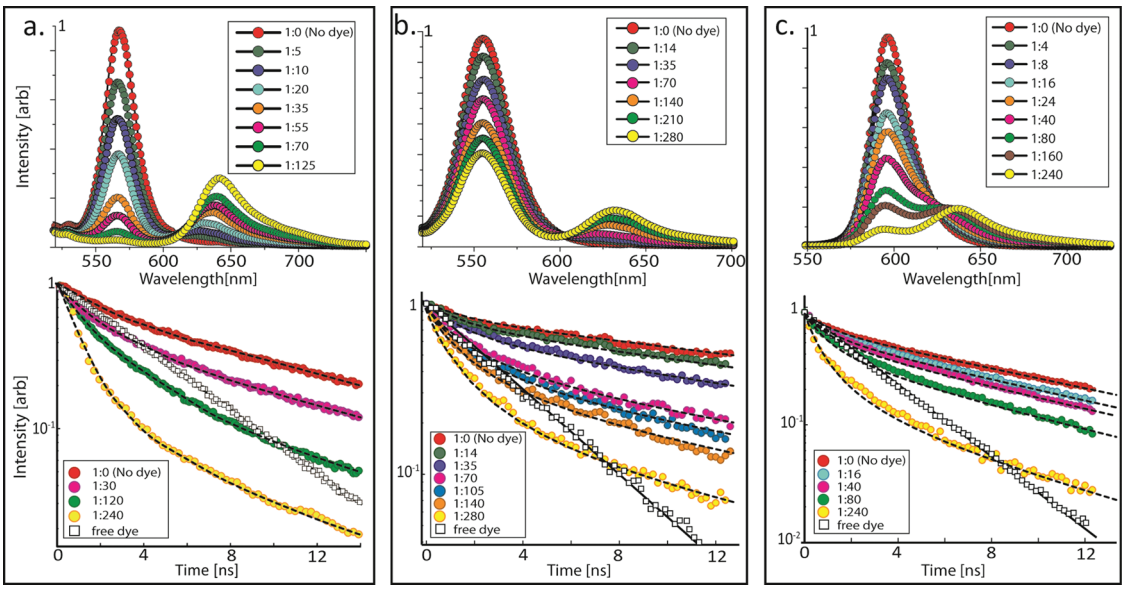

Figure 3. (a) Steady-state emission (top) and time-resolved spectra (bottom) for NPs with increasing ratios of Atto 590 to NP for (a) QD4.4, (b) DR93, and (c) RR. The existence of FRET between the NPs (donors) and the dye molecules (acceptors) is indicated both from steady-state emission, through quench of emission from the NPs and increase of emission from the dye, and from the temporal behavior, through the decrease in NP emission lifetime. Both phenomena increase with the addition of dye molecules per NP. Ratio of added dye molecules per NP, obtained from spectroscopic absorption measurements, is indicated in the legends. The temporal decay of free dye is portrayed in white squares and is fitted by a single exponential. Modeled fits for emission decays are portrayed in dashed black lines, showing very good agreement with the experimental results.

dye attached per NP can be attributed to the much lower surface dye concentration obtained in the elongated NP, leading to fewer acceptors in the proximity of the CdSe core and to less efficient FRET. The RR system also exhibits stronger quenching than the DR system despite their similar rod-like shell. This can be explained by considering that the inner rod transition dipole moment is spread throughout the particle, proximal to a larger surface area, and thus under similar surface concentration interacts with a larger number of acceptors.

Modeling the NP Conjugates Lifetime Behavior. In order to gain further information about the system, in particular regarding the dimensionality of the acceptor distribution, we employed a model based on a restricted geometries method,[24,25] which was shown to successfully describe the dependence of donors' emission time decay on the shape and density of the distribution of fluorophores in space. Within the model, the ensemble-averaged fluorescence intensity decay for the donor, $\phi(t)$, can be calculated using a probability density approach.[1,24] Averaging the single pair FRET rate term, $k_{FRET}(r) = \tau_D^{-1}(R_0/r)^6$, over all possible donor−acceptor configurations, the decay of an excited donor positioned at the origin as a function of time t is given by

$$\phi(t) = \exp(-k_D t)\exp(-c_A I) \qquad (1)$$

where k_D is the donor radiative decay rate ($k_D = \tau_D^{-1}$), c_A is the acceptor concentration, and I is the integration term,

$$I(t) = \int_V \left(1 - \exp\left[-\frac{t}{\tau_D}\left(\frac{R_0}{r}\right)^6\right]\right) dV \qquad (2)$$

carried out over the volume V of the region under consideration. This type of treatment was presented for spherical[24,26,27] and cylindrical systems[24,25] of different donor and acceptor distributions. The model can be formulated to treat a spherical core embedded in shells of different geometries, by treating the spherical core as a point dipole positioned in the center of the core.[28−30] The acceptors are assumed to reside in a shell whose shape is dictated by the shape of the NP, of specific thickness and distance from the surface of the particle. While the spherical core can be treated as a point dipole, this is not the case for the RR structure, where the core is rod-shaped and its transition dipole moment is directed along the main axis of the rod.[31] For describing the FRET of such systems, a complete quantum mechanical treatment extending beyond the Förster point dipole approximation should be employed,[28,32−34] which is not treated within the scope of the restricted geometries model. In order to obtain an approximate behavior of the system, we used a variation of the line dipole approximation,[35] where the overall dipole of the rod is partitioned into a sequence of fractional transition point dipoles linearly distributed along the main axis of the core−rod.

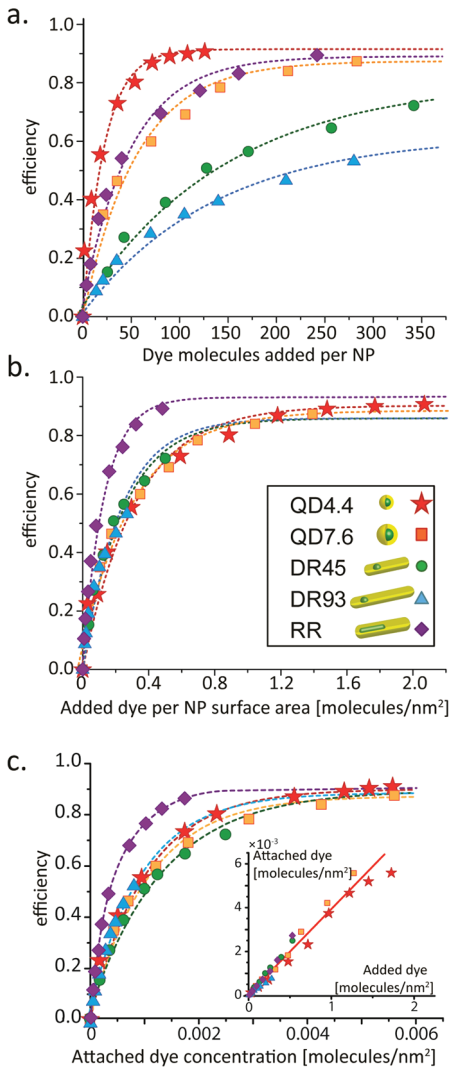

Figure 4. (a) FRET efficiency as a function of the number of dye molecules added per NP. For the same number of dye molecules per NP, higher efficiency is obtained as the volume of the NP decreases. The RR system exhibits remarkably higher efficiencies compared to the equivalent DR45 system under the same NP–dye ratios. (b) FRET efficiency as a function of dye molecules added per NP, normalized to the NP surface area. The normalized efficiencies for all systems with spherical cores overlap, while the RR system exhibits higher efficiencies for the same surface concentration. (c) FRET efficiency as a function of dye surface concentration extracted from the model. Under similar surface concentration systems exhibit similar efficiencies. Inset: Attached dye (from model) *vs* added dye (experimental) plot indicates a linear relation between added and attached dye molecules. The slope value of 3.8×10^{-3} indicates that for every 250 dye molecules added to the solution, approximately 1 gets attached to the NP surface. Dashed lines are guidance to the eye.

For additional details regarding the model, we refer the readers to the Supporting Information.

As can be seen in Figure 3, the agreement between the temporal decay measurements (symbols) and the modeled results under homogeneous distribution of the acceptors (dashed lines) is high, and the model captures the correct behavior for all measured systems (rods and dots) both at short times (first few nanoseconds) and at longer times.

Dimensionality Effect on FRET Efficiency. In order to establish the effect of dimensionality on the FRET process, we first examine the efficiency of FRET (η_{FRET}) for different systems, which can be easily obtained from the steady-state emission by

$$\eta_{FRET} = 1 - \frac{F_{DA}}{F_D} \quad (3)$$

where F_D is the emission intensity of the donor NPs, and F_{DA} the intensity measured for the donor–acceptor conjugates. Figure 4a shows the efficiencies obtained from the steady-state emission (symbols) as a function of the number of dye molecules added per NP. In general, the increase in efficiency as dye concentration increases is more pronounced as the size of the NP decreases. Again, assuming that the number of dye molecules attached to the NP is dictated by the amount of dye added per NP, this can be explained by the differences in the dye concentration on the NP surface of the different systems. At high numbers of dye molecules per NP, saturation of the efficiency is observed, though it does not approach unity, likely because of steric effects, which hinder the attachment of further acceptors at high surface concentration. As in these systems the R_0 values are quite close, the efficiency of the FRET process is mostly affected by the number of dye molecules attached in proximity to the NP core position. Thus in these systems the efficiency acts as an excellent indicator of the dye surface concentration.

Figure 4b shows the efficiency as a function of number of dye molecules added per unit surface area. Upon this normalization, the efficiency curves of all systems with spherical cores overlap, indeed indicating a correlation between the amounts of added and attached dye molecules per NP. In this set of experiments, where a complete ligand exchange was performed, it is reasonable to assume that the glutathione distribution is uniform, leading to a uniform distribution of attached dye. Under the assumption that the distribution of acceptors is directly governed by the NP shape, the restricted geometry model can be used for extracting the amount of acceptors per donor and the surface concentration from the efficiency, regardless of the NP shape. Figure 4c portrays the efficiency as a function of the extracted acceptors' surface density. Again, under such normalization the efficiency curves highly overlap, demonstrating the strong effect of local acceptor density in proximity of the donor on the efficiency. Plotting the extracted surface density against the dye added per surface area shows a linear relation between the two, indicating that under the experimental conditions, approximately for every 250 dye molecules added to the solution, one gets attached to the NP surface.

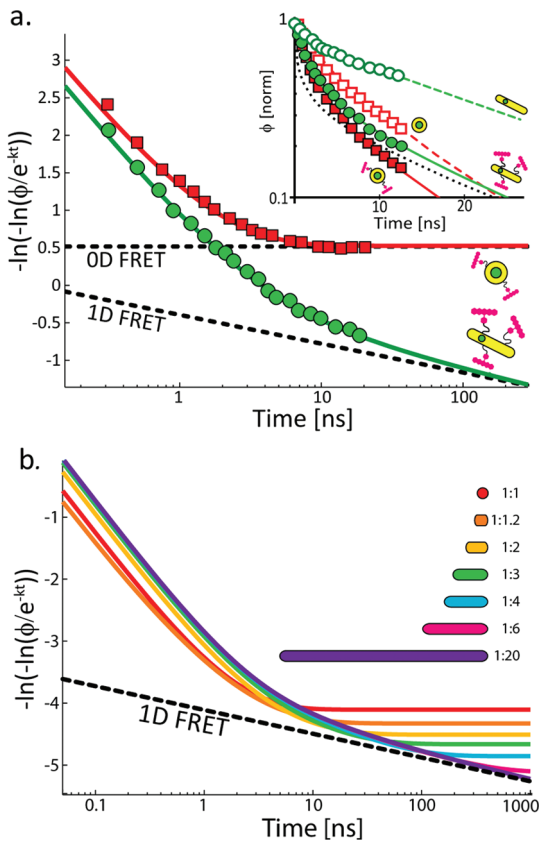

Figure 5. (a) Comparison of decay curves of QD4.4 spherical core/shell (red) and DR93 (green), obtained experimentally (symbols) and modeled using the restricted geometry model (lines) in a logarithmic plot. While at short times both systems decay exponentially, at long times QD4.4 shows no decay due to FRET (0D FRET), while DR93 converges to a 1D FRET decay curve. Inset shows the standard decay plot. Decay of bare NPs with no dyes attached is portrayed as dashed lines and open symbols, and decay of the conjugated NPs is shown as solid lines. (b) Modeled decay curve of NPs of different aspect ratios. Under the same conditions, the decay behavior at long times goes from 0D in the spherical system to 1D as the aspect ratio increases. A 1D decay becomes dominant at an aspect ratio of 6.

It should be accentuated that the FRET obtained from the system is related only to dye molecules attached to the NP surface and not to free dye molecules in the solution, as can be deduced both from the lack of FRET in nonconjugated systems and from the minor effect of dilution on the FRET behavior in conjugated systems, as described in detail in the Supporting Information (Figures S1 and S2).

In comparison to systems with spherical cores, the RR system exhibits a much higher increase in efficiency after normalization. This indicates that the FRET behavior of the RR system is different from all other systems examined in this study. This difference is attributed to the change in dimensionality of the emission center, leading to a different FRET interaction term, which falls beyond the Förster point dipole behavior, and to the interaction of the rod core dipole moment with a larger number of dye molecules on the NP surface. Recently published results by Hardzei *et al.*,[19] appearing after this paper was first submitted, indicated that upon attachment of a similar number of dye molecules per particle, the efficiency obtained for the QD system is higher than that obtained for the nanorod system. Yet, when examining their results after normalization of the efficiency to the number of dye molecules attached per surface area, higher efficiency per dye molecule attached per surface area is obtained for the elongated system in comparison with the spherical system, in agreement with the results obtained in this report. These results call for more detailed research of FRET in rod-like systems with elongated transition dipoles. The higher efficiency per surface concentration of elongated core systems is of particular interest for light-harvesting systems, as less dye is needed in order to obtain similar efficiencies of the energy transfer.

Dimensionality Effects in FRET Time Decay. While inspection of the FRET efficiency already reflects differences in the donor dimensionality, it is lacking sensitivity for extracting information regarding the long-range distribution of acceptors due to its high sensitivity to the local acceptor density. The FRET temporal decay, on the other hand, is dictated by the correlation between time and space, which is inherent to the FRET interaction (eq 2), and therefore it directly reflects the structural details. In general, in the case of multiple acceptors, the donor's decay can be described by a stretched exponent, $\phi(t) = e^{-(t/\tau_{rad})^{\beta}}$, where β reflects the dimensionality of the system. In the case of a system with restricted geometries, where the dimensionality of the acceptor distribution changes throughout the system, β approaches different values at different time regimes.[36] Due to the stretched exponential behavior, these crossovers are most apparent when the data are portrayed as a $-\log(-\log(\phi/\exp(-kt)))$ *vs* $\log(t)$ plot.

Figure 5a depicts the logarithmic plot for the experimental time decay (symbols) and the modeled results (lines) for QD4.4 (red, squares) as an example of a spherical system, and for DR93 (blue, circles), as an example of an elongated system, under similar surface concentration of ~0.006 dye molecule per nm^2 (inset shows the standard decay curve of the systems). While at short times ($t < k_{rad}R_0^6/r^6$, where r is the system radius) both systems exhibit exponential decay, at long times ($t > k_{rad}R_0^6/r^6$, which for these systems is ~8 ns), the two systems show distinctively different behavior. In the spherical QDs, the decay at long times becomes parallel to that of the bare particle fluorescent decay (Figure 4a inset, solid red), a behavior referred to as a 0D FRET. In the DR systems, on the other hand, the decay at long times converges to that of a 1D FRET system with equivalent acceptor concentration (dashed black line), thus capturing the elongated shape of the acceptor distribution of the rod system. Time decays of DR systems with similar thickness but

different aspect ratios calculated using the model indicate that already at an aspect ratio of 1:6 a pronounced 1D behavior is obtained (Figure 5b). Thus, the temporal decay at long times, which is still within the measurement scope, gives a direct indication of the dimensionality of the acceptor distribution.

CONCLUSIONS

The dimensionality of nanoparticles acting as donors can strongly affect the energy transfer characteristics in systems that consist of NPs conjugated to multiple acceptors. For nanorod donors of similar dimensions, going from a 0D to a 1D emission center leads to a large increase in FRET efficiency, making NP systems that go beyond the Förster point dipole limit highly sensitive single-particle probes for the nanoscale regime. The dimensionality and shape of the acceptor distribution, which is dictated by the NP geometry, are strongly manifested in the time decay curves and can be extracted from the experimental results by using a restricted geometries model. The ability to combine theoretical and experimental results and obtain such a detailed description of the FRET in nanosystems makes FRET lifetime not only an extremely sensitive analytical tool for extraction of the number of attached acceptors but, furthermore, also a unique probe for directly assessing the spatial distribution of acceptors in the vicinity of the nanoparticles, which can be used as an excellent real-time probe for inspecting the dynamics of attachment and conjugation processes, thus acting not only as a "nanoruler" for distances but also as a concentration indicator in the nanoscale regime.

METHODS

NP Synthesis. CdSe/CdS core/shell NPs were prepared following previously reported procedures for seeded growth. Briefly, CdSe spherical cores were synthesized according to ref 21 by swiftly injecting a stock solution of Se dissolved in trioctylphosphine (TOP) into a three-neck flask containing CdO in tri-*n*-octylphosphine oxide (TOPO) and *n*-octadecylphosphonic acid (ODPA) at 360 °C under an Ar atmosphere. In order to obtain diameters of 1.9−2.2 nm, the synthesis was immediately quenched by swift injection of cold TOP. The crude solution was then washed with methanol to remove excess ligands. The concentration of cores in the solution was calculated from absorption measurements and then divided into batches for further synthesis. CdSe nanorods were synthesized according to ref 37. In this synthesis, a Cd stock solution, prepared by dissolving $Cd(CH_3)_2$ in tributylphosphine (TBP), was added dropwise to a flask containing TOPO and tetradecylphosphonic acid heated under an argon atmosphere to 360 °C. A minute later a solution of Se in TBP was rapidly injected, and the solution was cooled to 290 °C. The reaction was stopped by rapid cooling after 15 min to yield rods of 9 nm × 2.2 nm. The crude reaction mixture was diluted with toluene. Methanol was added in order to precipitate the nanorods with the aid of centrifugation.

CdSe/CdS spherical core/shell NPs were prepared using the SILAR method.[20] In a typical synthesis, CdSe cores dissolved in chloroform are added to a three-neck flask containing 1-octadecene and octadecylamine at 50 °C. The system is then allowed to heat under vacuum to 100 °C for 1 h in order to remove the chloroform and then transferred to an argon atmosphere. The system was then heated to 200 °C, and precursor solutions of $Cd(Ac)_2$ in TOP and elemental sulfur in TOP (both 0.1 M) were added dropwise sequentially with a time interval of 10 min between each injection. The amount of precursor added in each step was calculated according to ref 20, and the number of additions was determined according to the desired shell size. The crude reaction mixture was diluted with toluene. Methanol was added, and the solution was centrifuged in order to precipitate the NPs. CdSe/CdS DRs were prepared according to the seeded growth synthesis reported in ref 21, and RRs were prepared according to the synthesis reported in ref 22. In a typical synthesis, elemental sulfur was dissolved in TOP and added to CdSe NPs (either dots or rods) synthesized as described above. The solution of CdSe NPs and sulfur in TOP was swiftly injected into a three-neck flask containing TOPO, ODPA, hexylphosphonic acid, and CdO at 360 °C. The nanocrystals were grown for 8 min after the injection. After cooling, the crude solution was dissolved in toluene, and methanol was added in order to precipitate the NPs and remove excessive surfactants. Rods with different lengths of CdS shells were obtained by changing the ratio of precursors to CdSe cores, as was previously reported.[21]

Transmission electrons microscope characterization was performed using a Tecnai T12 G2. Absorption spectra were collected using a JASCO V-570 UV−vis−near IR spectrophotometer, and emission measurements were collected using a Varian Cary Eclipse fluorometer. Extinction coefficient values of the NPs were calculated using a previously reported method.[38]

Conjugation to the Dye Molecules. The aqueous fraction containing the NPs with glutathione ligands was collected and transferred into Millipore-Amicon Ultra centrifugal filters of 10K for QDs or of 100K for nanorods. The samples were washed several times and centrifuged at 4000 rpm for 40 min to remove excess glutathione and base, until a pH of 6 was obtained, in which a conjugation reaction to the dye molecules can be achieved. Atto dye 590 NHS ester (2.5×10^{-1} mg) was dissolved in 2 mL of dimethylformamide, and different volumes of the solution (ranging from 3 to 120 μL) were added to 100 μL of aqueous solutions of NPs. The solutions were then stirred for 3 h at room temperature. The overall process is portrayed in Figure 1c.

Lifetime Measurements. A series of NP−dye solutions of different dye concentrations in water were diluted to low concentrations to eliminate FRET between adjacent nonconjugated NPs or dye molecules. A cuvette containing each of the solutions was excited by a mode-locked doubled Ti:sapphire laser at 450 nm (Coherent Mira) with pulse width of 120 fs and repetition rate of 76 MHz. The laser was horizontally polarized, and the excitation power was attenuated by a variable neutral density filter. The laser beam with an average power of 1 mW was focused to a 2 mm spot. The emission from the sample was collected at a right angle, filtered with a short pass filter to suppress the fundamental excitation light of the laser, dispersed using a monochromator (Acton SpectraPro-300i), and detected with an iCCD (LaVision PicoStar HR).

Conflict of Interest: The authors declare no competing financial interest.

Acknowledgment. The research leading to these results has received funding from the European Research Council under the European Union's Seventh Framework Programme (FP7/2007−2013)/ERC grant agreement no. 246841. U.B. thanks the Alfred and Erica Larisch Memorial Chair. A.S. is grateful for a fellowship given by The Eshkol Foundation, administered by Israel Ministry of Science. S.H. and A.S. contributed equally to

this work, designed and performed experiments, analyzed data, and wrote the manuscript. A.S. developed and performed the restricted geometries modeling; I.H. performed spectroscopic measurements; U.B. supervised the project and wrote the manuscript.

Supporting Information Available: 1. Control experiments, 2. Modeling NP FRET behavior using restricted geometries approach, 3. Utilization of separation methods for removal of free dye molecules, 4. Ligand exchange procedure. This material is available free of charge *via* the Internet at http://pubs.acs.org.

REFERENCES AND NOTES

1. Förster, T. Experimentelle Und Theoretische Untersuchung Des Zwischenmolekularen Ubergangs Von Elektronenanregungsenergie. *Z Naturforsch. A: Astrophys. Phys. Phys. Chem.* **1949**, *4*, 321–327.
2. Förster, T. 10th Spiers Memorial Lecture, Transfer Mechanisms of Electronic Excitation. *Discuss Faraday Soc.* **1959**, *27*, 7–17.
3. Clapp, A. R.; Medintz, I. L.; Mattoussi, H. Forster Resonance Energy Transfer Investigations Using Quantum-Dot Fluorophores. *ChemPhysChem* **2006**, *7*, 47–57.
4. Rogach, A. L.; Klar, T. A.; Lupton, J. M.; Meijerink, A.; Feldmann, J. Energy Transfer with Semiconductor Nanocrystals. *J. Mater. Chem.* **2009**, *19*, 1208–1221.
5. Alivisatos, A. P.; Gu, W. W.; Larabell, C. Quantum Dots as Cellular Probes. *Ann. Rev. Biomed. Eng.* **2005**, *7*, 55–76.
6. Sandoghdar, V.; Seelig, J.; Leslie, K.; Renn, A.; Kuhn, S.; Jacobsen, V.; van de Corput, M.; Wyman, C. Nanoparticle-Induced Fluorescence Lifetime Modification as Nanoscopic Ruler: Demonstration at the Single Molecule Level. *Nano Lett.* **2007**, *7*, 685–689.
7. Gill, R.; Willner, I.; Shweky, I.; Banin, U. Fluorescence Resonance Energy Transfer in Cdse/Zns-DNA Conjugates: Probing Hybridization and DNA Cleavage. *J. Phys. Chem. B* **2005**, *109*, 23715–23719.
8. Willner, I.; Willner, B. Biomolecule-Based Nanomaterials and Nanostructures. *Nano Lett.* **2010**, *10*, 3805–3815.
9. Resch-Genger, U.; Grabolle, M.; Cavaliere-Jaricot, S.; Nitschke, R.; Nann, T. Quantum Dots Versus Organic Dyes as Fluorescent Labels. *Nat. Methods* **2008**, *5*, 763–775.
10. Mattoussi, H.; Sapsford, K. E.; Pons, T.; Medintz, I. L. Biosensing with Luminescent Semiconductor Quantum Dots. *Sensors* **2006**, *6*, 925–953.
11. Medintz, I. L.; Mattoussi, H. Quantum Dot-Based Resonance Energy Transfer and Its Growing Application in Biology. *Phys. Chem. Chem. Phys.* **2009**, *11*, 17–45.
12. Nikiforov, T. T.; Beechem, J. M. Development of Homogeneous Binding Assays Based on Fluorescence Resonance Energy Transfer between Quantum Dots and Alexa Fluor Fluorophores. *Anal. Biochem.* **2006**, *357*, 68–76.
13. Sapsford, K. E.; Granek, J.; Deschamps, J. R.; Boeneman, K.; Blanco-Canosa, J. B.; Dawson, P. E.; Susumu, K.; Stewart, M. H.; Medintz, I. L. Monitoring Botulinum Neurotoxin a Activity with Peptide-Functionalized Quantum Dot Resonance Energy Transfer Sensors. *ACS Nano.* **2011**, *5*, 2687–2699.
14. Kotov, N. A.; Lee, J.; Govorov, A. O. Bioconjugated Superstructures of Cdte Nanowires and Nanoparticles: Multistep Cascade Forster Resonance Energy Transfer and Energy Channeling. *Nano Lett.* **2005**, *5*, 2063–2069.
15. Franzl, T.; Koktysh, D. S.; Klar, T. A.; Rogach, A. L.; Feldmann, J.; Gaponik, N. Fast Energy Transfer in Layer-by-Layer Assembled Cdte Nanocrystal Bilayers. *Appl. Phys. Lett.* **2004**, *84*, 2904–2906.
16. Patra, A.; Sadhu, S. Donor-Acceptor Systems: Energy Transfer from Cds Quantum Dots/Rods to Nile Red Dye. *ChemPhysChem* **2008**, *9*, 2052–2058.
17. Sadhu, S.; Tachiya, M.; Patra, A. A Stochastic Model for Energy Transfer from Cds Quantum Dots/Rods (Donors) to Nile Red Dye (Acceptors). *J. Phys. Chem. C* **2010**, *114*, 2842–2842.
18. Artemyev, M.; Ustinovich, E.; Nabiev, I. Efficiency of Energy Transfer from Organic Dye Molecules to Cdse-Zns Nanocrystals: Nanorods versus Nanodots. *J. Am. Chem. Soc.* **2009**, *131*, 8061–8065.
19. Hardzei, M.; Artemyev, M.; Molinari, M.; Troyon, M.; Sukhanova, A.; Nabiev, I. Comparative Efficiency of Energy Transfer from Cdse-Zns Quantum Dots or Nanorods to Organic Dye Molecules. *ChemPhysChem* **2012**, *13*, 330–335.
20. Li, J. J.; Wang, Y. A.; Guo, W. Z.; Keay, J. C.; Mishima, T. D.; Johnson, M. B.; Peng, X. G. Large-Scale Synthesis of Nearly Monodisperse Cdse/Cds Core/Shell Nanocrystals Using Air-Stable Reagents *via* Successive Ion Layer Adsorption and Reaction. *J. Am. Chem. Soc.* **2003**, *125*, 12567–12575.
21. Carbone, L.; Nobile, C.; De Giorgi, M.; Sala, F. D.; Morello, G.; Pompa, P.; Hytch, M.; Snoeck, E.; Fiore, A.; Franchini, I. R.; *et al.* Synthesis and Micrometer-Scale Assembly of Colloidal Cdse/Cds Nanorods Prepared by a Seeded Growth Approach. *Nano Lett.* **2007**, *7*, 2942–2950.
22. Sitt, A.; Salant, A.; Menagen, G.; Banin, U. Highly Emissive Nano Rod-in-Rod Heterostructures with Strong Linear Polarization. *Nano Lett.* **2011**, *11*, 2054–2060.
23. Medintz, I. L.; Konnert, J. H.; Clapp, A. R.; Stanish, I.; Twigg, M. E.; Mattoussi, H.; Mauro, J. M.; Deschamps, J. R. A Fluorescence Resonance Energy Transfer-Derived Structure of a Quantum Dot-Protein Bioconjugate Nanoassembly. *Proc. Natl. Acad. Sci. U. S. A.* **2004**, *101*, 9612–9617.
24. Blumen, A.; Klafter, J.; Zumofen, G. Influence of Restricted Geometries on the Direct Energy-Transfer. *J. Chem. Phys.* **1986**, *84*, 1397–1401.
25. Farinha, J. P. S; Spiro, J. G.; Winnik, M. A. Dipole-Dipole Electronic Energy Transfer: Fluorescence Decay Functions for Arbitrary Distributions of Donors and Acceptors in Systems with Cylindrical Symmetry. *J. Phys. Chem. B* **2004**, *108*, 16392–16400.
26. Yekta, A.; Winnik, M. A.; Farinha, J. P. S; Martinho, J. M. G. Dipole-Dipole Electronic Energy Transfer: Fluorescence Decay Functions for Arbitrary Distributions of Donors and Acceptors. II. Systems with Spherical Symmetry. *J. Phys. Chem. A* **1997**, *101*, 1787–1792.
27. Tcherkasskaya, O.; Gronenborn, A. M.; Klushin, L. Excluded Volume Effect within the Continuous Model for the Fluorescence Energy Transfer. *Biophys. J.* **2002**, *83*, 2826–2834.
28. Scholes, G. D.; Beljonne, D.; Curutchet, C.; Silbey, R. J. Beyond Forster Resonance Energy Transfer in Biological and Nanoscale Systems. *J. Phys. Chem. B* **2009**, *113*, 6583–6599.
29. Scholes, G. D.; Curutchet, C.; Franceschetti, A.; Zunger, A. Examining Forster Energy Transfer for Semiconductor Nanocrystalline Quantum Dot Donors and Acceptors. *J. Phys. Chem. C* **2008**, *112*, 13336–13341.
30. Baer, R.; Rabani, E. Theory of Resonance Energy Transfer Involving Nanocrystals: The Role of High Multipoles. *J. Chem. Phys.* **2008**, 128.
31. Shabaev, A.; Efros, A. L. 1d Exciton Spectroscopy of Semiconductor Nanorods. *Nano Lett.* **2004**, *4*, 1821–1825.
32. Wong, C. Y.; Curutchet, C.; Tretiak, S.; Scholes, G. D. Ideal Dipole Approximation Fails to Predict Electronic Coupling and Energy Transfer between Semiconducting Single-Wall Carbon Nanotubes. *J. Chem. Phys.* **2009**, 130.
33. Schrier, J.; Wang, L. W. Shape Dependence of Resonant Energy Transfer between Semiconductor Nanocrystals. *J. Phys. Chem. C* **2008**, *112*, 11158–11161.
34. Andrews, D. L.; Curutchet, C.; Scholes, G. D. Resonance Energy Transfer: Beyond the Limits. *Laser Photonics Rev.* **2011**, *5*, 114–123.
35. Beenken, W. J. D.; Pullerits, T. Excitonic Coupling in Polythiophenes: Comparison of Different Calculation Methods. *J. Chem. Phys.* **2004**, *120*, 2490–2495.
36. Drake, J. M.; Klafter, J.; Levitz, P. Chemical and Biological Microstructures as Probed by Dynamic Processes. *Science* **1991**, *251*, 1574–1579.
37. Peng, X. G.; Manna, L.; Yang, W. D.; Wickham, J.; Scher, E.; Kadavanich, A.; Alivisatos, A. P. Shape Control of Cdse Nanocrystals. *Nature* **2000**, *404*, 59–61.
38. Shaviv, E.; Salant, A.; Banin, U. Size Dependence of Molar Absorption Coefficients of Cdse Semiconductor Quantum Rods. *ChemPhysChem* **2009**, *10*, 1028–1031.